Semi-autonomous Teleimpedance Based on Visual Detection of Object Geometry and Material and its Relation to Environment

Siegemund, G.; Díaz Rosales, A.; Glodde, Arne; Dietrich, Franz; Peternel, L.

DOI
10.1109/Humanoids58906.2024.10769858

Publication date
2024

Document Version
Final published version

Published in
Proceedings of the IEEE-RAS 23rd International Conference on Humanoid Robots (Humanoids 2024)

2024 IEEE-RAS 23rd International Conference on Humanoid Robots (Humanoids)
Nancy, France. November 22-24, 2024

2024 IEEE-RAS 23rd International Conference on Humanoid Robots (Humanoids) | 979-8-3503-7357-8/24/$31.00 ©2024 IEEE | DOI: 10.1109/Humanoids58906.2024.10769858

Semi-autonomous Teleimpedance Based on Visual Detection of Object Geometry and Material and its Relation to Environment

Georg Siegemund[1,2], Alejandro Diaz Rosales[1,3], Arne Glodde[2], Franz Dietrich[2], and Luka Peternel[1]

***Abstract*— This paper presents a method for semi-autonomous teleimpedance where the control is shared between the human operator and the robot. The human commands the position of the teleoperated robotic arm end-effector while the robot autonomously adjusts the impedance depending on the object with which the end-effector interacts. We developed a vision system that calculates the appropriate robot stiffness based on the detected object geometry and material and object's relation to the environment. This system uses an RGB-D camera near the robot's end-effector to capture different perspectives of the scene. To validate the proposed method, we conducted experiments on a teleoperation system where a Force Dimension Sigma7 haptic device was used to operate a KUKA LBR iiwa robotics arm. At the same time, the Intel RealSense D455 depth camera provided the visual input. We examined two practical tasks: engaging with bolts on a plate and polishing a stripe.**

I. Introduction

Due to their versatility and diverse capabilities, humanoid robots are indispensable tools for performing complex and hazardous tasks, such as disaster response [1]. In most cases, we prefer the humanoid robot to autonomously execute their tasks as much as possible. Nevertheless, human involvement is often still desired or required due to the complexity of the task and the lack of robot cogitative capabilities. A key technology that enables human-in-the-loop robot control and teaching is teleoperation [2]. An operator can control a remote robot through interfaces and perform tasks in unstructured and unpredictable environments.

For robotic manipulators, it is challenging to physically interact in unstructured and unpredictable environments, as they lack the human ability to analyze new objects and adapt the interaction control. Humans are very good at estimating objects by analyzing the structure and material of the object. Based on that, they can then adapt their arm endpoint stiffness to perform an effective physical interaction [3]. For example, if interacting with a fragile part of an object, the stiffness can be lowered to ensure it does not break. When requiring more strength on a rigid part of the object, the stiffness can be increased to be more forceful.

To enhance the classic teleoperation of a robotic manipulator with impedance control, the concept of teleimpedance was developed [4]. Teleimpedance enables the operator to control the impedance remotely with an additional command channel [5]. To this end, various stiffness command interfaces have been developed, such as hand-grip-sensors [6], electromyography (EMG) [7]–[12], visual muscle activity estimation [13], buttons/sliders [14]–[16], and haptic interface wiggling [17] and perturbations [18]. While stiffness command interfaces enable direct human control over the remote robot impedance, the trade-off is that they add extra task load on the operator.

Fig. 1. Experiment setup including KUKA LBR iiwa robotic arm controlled by a human operator using Force Dimension Sigma.7 haptic device. Intel RealSense D455 depth camera is mounted close to the robot end-effector, and its information is used for autonomous adjustments of robot impedance. The image shows an example of a task where a stripe needs to be polished.

Many studies successfully investigated the possibilities of autonomous impedance controllers. For example, machine learning methods such as reinforcement learning [19] or learning from demonstration [20], [21] enable the robot to learn and reproduce impedance regulation skills. Nevertheless, these methods do not apply to real-time teleoperation where human needs quick online adjustments. The limiting factor of machine learning methods is that they rely on the learned impedance trajectory, which may not adapt fast enough when the operator changes the position trajectory rapidly in real-time.

Alternatively, adaptive impedance controllers based on haptic feedback can achieve trajectory-independent control. The approach closely aligns with human behaviour, relying on haptic senses to estimate the interaction and adjust the impedance [22]–[24]. Nevertheless, physical interaction between the robot and the environment before adjusting impedance can be dangerous in situations where the envi-

[1]Cognitive Robotics, Delft University of Technology, Delft, The Netherlands (e-mail: g.siegemund@tudelft.nl, a.diazrosales@tudelft.nl, l.peternel@tudelft.nl)

[2]Handling and Assembly Technology Research, Fakultät V, Technische Universität Berlin, Berlin, Germany (e-mail: g.siegemund@campus.tu-berlin.de, arne.glodde@tu-berlin.de, f.dietrich@tu-berlin.de)

[3]European Organization for Nuclear Research (CERN), Meyrin, Switzerland

ronment is unknown, unstable, or fragile. The robot risks damaging the object when the impedance is not adapted to the object in time. In such instances, the impedance should be adjusted to the given object before the initial contact.

To this end, a recent study in [25] introduced a semi-autonomous teleimpedance method where the remote robot can estimate the impedance on its own using computer vision, which estimates the material of the object and, depending on the material, sets an impedance for the robot before the object is touched. Nevertheless, the key drawback of that method is that object geometry and its relation to the environment were neglected. For example, a thin metal can be more fragile than a thick glass, even though glass as a material tends to be more fragile in general. Furthermore, when a robot needs to bend an object to a specific angle, the required force depends not only on the material but also on the overall shape and the point at which the force is applied. Incorporating object geometry and its relation to the environment for semi-autonomous teleimpedance remains an important open research challenge.

The research in this paper aims to address this gap in the current state of the art by proposing a new method to efficiently estimate the appropriate robot's impedance for interacting with an object. This method takes into account the object's shape, material properties, and its interaction with the rest of the environment. To validate the proposed method, we conduct several experiments on a setup involving Force Dimension Sigma.7 haptic device that controls the motion of KUKA LBR iiwa remote robotic manipulator and Intel RealSense D455 depth camera mounted on the robot to estimate object properties for impedance regulation (see Fig. 1). We examine tasks such as bolt engagement and surface polishing on different objects.

The method is shown in Fig. 2 and is composed of two main parts: object-aware impedance control (Sec. II) and computer vision algorithm (Sec. III). The impedance estimation module (Sec. II-A) of the object-aware impedance control part draws information about object geometry, material, and its relation of object to the environment from the computer vision algorithm using the camera mounted on the robot end-effector. The geometry-aware stiffness strategy enables adapting impedance calculation mode based on the relation of the object to the environment (e.g., how it is pivoted/mounted). The impedance command module (Sec. II-B) of the object-aware impedance control part uses the information about the object from the impedance estimation module to adapt and command the stiffness to the remote robot end-effector. The object detection modules (Sec. III) of the computer vision part provide the objects/environment information according to the camera input, where the object geometry, its material, and its relation to the environment are recognised. We estimate the object and its relation to the environment before the robot enters into contact to be proactive and not reactive.

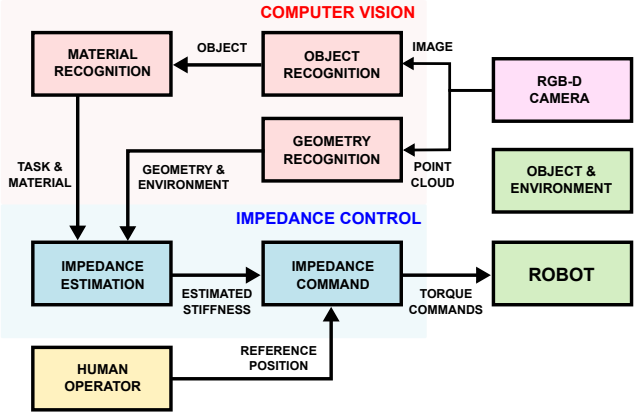

Fig. 2. Block scheme of the proposed method for semi-autonomous teleimpedance, which is composed of two main parts: geometry-aware impedance control (blue) and computer vision (red). The human operator controls the position of the remote robot end-effector, while the autonomous system controls its stiffness based on the detected object properties and its relation to the environment.

II. Object-Aware Impedance Control

The object-aware impedance control part covers two modules. The impedance estimation module estimates the appropriate impedance of the robot for the interaction with a specific object based on the data from computer vision. The impedance command module ensures that the estimated impedance is properly commanded to the remote robot in real-time, while the operator commands the position.

A. Impedance Estimation Module

The robot estimates the impedance autonomously based on the information about the object properties, which is obtained from the computer vision part (Sec. III). The key part of the regulated impedance is stiffness, while the damping is adjusted to maintain the controller's stability. To determine a suitable robot stiffness in different possible robot positions, we need to analyse the object geometry and material. Let us examine the following scenario. We need to produce a force on the surface of a rectangular object, such as a plate. The robot end-effector needs to interact with the plate perpendicularly to the object's surface, thus stiffness needs to be adjusted in that direction while maintaining high stiffness in the other axes to ensure precise positioning. Examples of such a scenario are common tasks such as polishing a plate [26]–[28] or screwing bolts [14], [29].

The adjustments of stiffness in a perpendicular direction depend on the geometry and properties of the object. If the plate is thin or made of a fragile material, the stiffness should ideally be lower to ensure we do not bend it too much. If it is pivoted on one side and free on the other, the stiffness should be ideally adjusted based on the lever arm, as the sections farther from the pivot can bend more easily. Consequently, the geometry and material inherently shape the stiffness calculation by guiding the direction in which adjustments are required, along with determining the minimum and maximum stiffness.

To assess the appropriate stiffness, we created a function that depends on the combination of object geometry and its

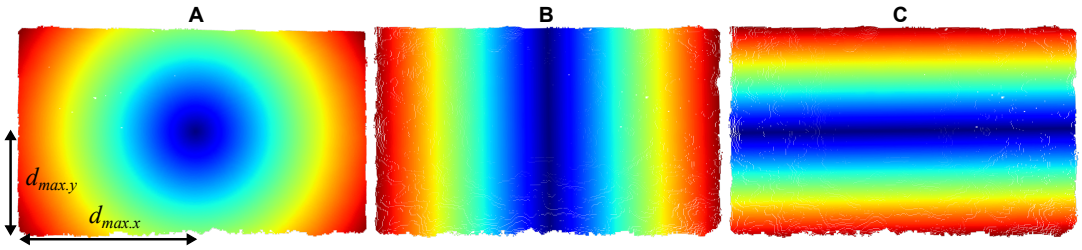

Fig. 3. Heatmap depicting stiffness values on the surface of an object (e.g., plate) during force production tasks, depending on the configuration of environment support: supported on all four edges (A), supported on left and right edges (B) and supported on top and bottom edges (C). Red color indicates high stiffness, while blue color indicates low stiffness.

material information obtained from computer vision. This function is defined by the maximum distance to the weakest spot of the object, as well as the maximum and minimum stiffness. Depending on the object's geometry and its relation to the environment (i.e., configuration of environment support), the point of minimal stiffness is located differently. Returning to the scenario of force production on a rectangular object (e.g., a plate) and assuming the environment support is situated beneath the plate's borders, the minimum stiffness is essentially at the centre of the plate.

The stiffness function depends on the object's geometry and changes based on the location and the amount of support the environment provides in different positions. Fig. 3 shows examples where the environment supports a plate differently. Image A shows a case when support is on all four sides of the object. Image B shows a case where the environment supports the object on the left and right ends, while image C shows a case where support is provided on the top and bottom ends. The red color indicates higher object stiffness closer to the supports since the lever arm is smaller and an external force does not easily bend the object. The blue color indicates lower object stiffness farther from the support since the lever arm becomes larger and the object can more easily bend. Higher stiffness is indicated near the plate borders, corresponding to the object's proximity to the support, whereas lower stiffness is desired at the centre of the plate.

For the case where the environment on both sides supports the object, the stiffness can be calculated as translational and rotational elements of each principal axis i of the object frame as

$$K^o_{ii} = \frac{K_{max.i}}{d_{max.i}} \cdot d_i > K_{min.i}. \tag{1}$$

When the support is only on one side, the stiffness can be calculated as

$$K^o_{ii} = \frac{K_{max.i}}{d_{max.i}} \cdot (d_{max.i} - d_i) > K_{min.i}, \tag{2}$$

where K^o_{ii} are the diagonal elements of the stiffness matrix $\boldsymbol{K}^o \in \mathbb{R}^{3\times3}$ calculated for the object and superscript ^{o} indicates that it is in the object frame. K_{min} and K_{max} are the maximum and minimum stiffness parameters, respectively, while $\boldsymbol{d}_{max} \in \mathbb{R}^3$ is the maximum distance parameter depending on object geometry. When the object (e.g., plate) is supported by the environment on both ends, d_{max} is the distance from the centre point to the borders. When it is clamped on one side only, d_{max} is the distance between the clamped position and the endpoint of the object on the other side. Lastly, d marks the current distance of the robot position from the weakest point, e.g., centre point for two-sided support or from the clamp for one-side support.

The detected object material determines the maximum and minimum stiffness parameters. For example, for stiffer materials, these are higher than for softer ones. Note that in (1) and (2), we assume the material stiffness is uniform, and thus the relationship is linear. If the material exhibits a non-linear relationship, the non-linear function can be employed instead.

B. Impedance Command Module

The derived object geometry-dependent stiffness from (1) or (2) is then used to command the stiffness of the robot end-effector that interacts with it at different positions. Thus, the stiffness has to be adapted when the robot moves with respect to the object's position. To ensure a smooth transition in the commanded stiffness, we use the following first-order integration function:

$$K_{ii}(t+dt) = \begin{cases} K^o_{min.i}, & \text{if } K_{ii}(t) < K^o_{min.i} \\ K^o_{max.i}, & \text{if } K_{ii}(t) > K^o_{max.i} \\ K^o_{ii} + e^{-g}(K_{ii}(t) - K^o_{ii}), & \text{if otherwise} \end{cases} \tag{3}$$

where K^o_{ii} is the ii-the element of the desired calculated stiffness matrix from (1) or (2), $K_{ii}(t)$ the currently commanded stiffness of the robot, and $K_{ii}(t+dt)$ the updated commanded stiffness in the next sample time. Note that depending on the relative difference between K^o_{ii} and $K_{ii}(t)$, the function transforms in either falling ($K^o_{ii} < K_{ii}(t)$) or raising ($K^o_{ii} > K_{ii}(t)$). Parameter g controls the adaption rate and can be tuned depending on the task and conditions. The following considerations should be taken into account when setting g. For example, rapid continuous changes in robot stiffness may be too quick for the operator to adapt to when commanding the end-effector position. On the other hand, substantial step changes can induce instability or dangerous situations when force might increase suddenly.

Stiffness elements from (1) and (2) adapted through (3) then form the commanded stiffness matrix $\boldsymbol{K}^o \in \mathbb{R}^{3\times3}$ in the object frame. Note that if the object frame and the robot base frame are not aligned, we must transform the object stiffness

matrix $\boldsymbol{K}^o$ into the robot base frame where the controller is operating as $\boldsymbol{K}^b = \boldsymbol{R}\boldsymbol{K}^o\boldsymbol{R}^T$, where $\boldsymbol{K}^b \in \mathbb{R}^{6\times6}$ is the stiffness matrix in the robot base frame and $\boldsymbol{R} \in \mathbb{R}^{3\times3}$ is the rotation matrix between the object frame and the robot base frame, which can be derived using information from the camera. While $\boldsymbol{K}^o$ is typically diagonal when the object frame is defined along the principal axes of the object, the stiffness matrix $\boldsymbol{K}^b$ becomes a non-diagonal matrix.

The autonomous stiffness adaption and the operator-commanded reference position are used to control the remote robot's physical interactive behaviour according to the impedance control law [30] as

$$\boldsymbol{f} = \boldsymbol{K}^b(\boldsymbol{x}_r - \boldsymbol{x}) + \boldsymbol{D}(\dot{\boldsymbol{x}}_r - \dot{\boldsymbol{x}}), \tag{4}$$

where $\boldsymbol{f} \in \mathbb{R}^6$ is the end-effector force/torque of the robot engaging the environment, $\boldsymbol{x}_r \in \mathbb{R}^6$ and $\boldsymbol{x} \in \mathbb{R}^6$ the reference and actual robot end-effector position, respectively, while $\boldsymbol{K}^b \in \mathbb{R}^{6\times6}$ and $\boldsymbol{D} \in \mathbb{R}^{6\times6}$ the Cartesian Stiffness and damping matrix, respectively. All these variables are expressed in the robot base frame. The damping matrix is dependent on the current stiffness matrix according to a double diagonalisation design [31] as

$$\boldsymbol{D} = 2 \cdot \boldsymbol{Q}\boldsymbol{D}_\xi \cdot \sqrt{\boldsymbol{K}_0} \cdot \boldsymbol{Q}^T, \tag{5}$$

where $\boldsymbol{Q} \in \mathbb{R}^{6\times6}$ and $\boldsymbol{\Sigma} \in \mathbb{R}^{6\times6}$ are the eigenvectors and eigenvalues of the eigendecomposition of the stiffness matrix with $\boldsymbol{K} = \boldsymbol{Q}\boldsymbol{\Sigma}\boldsymbol{Q}^T$, while $\boldsymbol{D}_\xi \in \mathbb{R}^{6\times6}$ contains the damping ratios set to 0.7. Finally, the commanded torque was calculated as $\boldsymbol{\tau} = \boldsymbol{J}(\boldsymbol{q})^T\boldsymbol{f}$, where $\boldsymbol{J} \in \mathbb{R}^{6\times7}$ is the robot Jacobian matrix and $\boldsymbol{q} \in \mathbb{R}^7$ is joint configuration vector.

III. Computer Vision for Object Estimation

To properly determine the stiffness of the object and adjust the robot to interact with it, we must estimate the object's properties. To do so, we utilize computer vision techniques. An overview of this part is shown in Fig. 2, which involves three key modules: 1) recognition of the object related to the task (object recognition), 2) the detection of the material of the object (material detection), and 3) the recognition of its shape and relation to the environment (geometry recognition). The input information needed for these modules is the RGB-D images from a camera mounted on the robot. The setup with a camera mounted close to the robot end-effector (Fig. 1) enables the robot to change the point of view to observe the object and the scene from different perspectives.

A. Object recognition module

The object recognition module takes the RGB images of the camera and processes them using YOLOv8 (You Only Look Once) [32], where the model was trained with the expected objects. In the first step, we acquired various images to be used as a dataset by placing and recording objects in various locations in the environment. The images were taken with the same camera used later in the experiments under different lighting conditions to ensure the model robustness to such variations. The collected images for the training dataset were then labeled based on the object classes, e.g., plates, stripes, etc. For labeling, we used Roboflow [33]. Additionally, annotations were applied to increase the number of images and make the model more robust. The created dataset was split into a training subset (80% of the dataset), a testing subset (10% of the dataset), and a validation subset (10% of the dataset). We then used the dataset for the model training.

B. Material recognition module

The material recognition module takes the mask provided by the object detector and analyzes the segmented object, adding the identified material of such object. A neural network trained on Materials in Context Database (MINC) [34] created a model to recognize the material. The material database provides images for 25 categories with pixel-wise annotations for each image. The goal of the model is to distinguish common materials such as wood and metal.

In the first step, the dataset's images were sorted depending on the label. To facilitate the classification task, the image requires adaptation to reveal the labeled material of interest exclusively. For this reason, we prepared a dataset by cropping the image with 40x40 px window for each annotated pixel in the image, with the annotated pixel as a centre point. The generated dataset included 135,000 images of crops showing wood and 150,000 showing metal. The prepared images were loaded and connected to the corresponding label.

After preparing the dataset, we transformed the images into tensors and performed the training with PyTorch. Therefore, the Vision Transformer (ViT) image processor was used. Additionally, before the transformation to the tensor, the images were transformed to RGB images and normalized. With the resulting prepared dataset, the actual training process started. For each used material we conducted preliminary experiments to estimate how much force could be applied without bending the object beyond an acceptable margin. Afterwards, the model identified the object material from the given image and got its Young's modulus. With the bending margin and Young's module, we then determined the minimum and maximum allowable stiffness values ($K_{min.i}$ and $K_{max.i}$) for interacting with the object.

C. Geometry recognition module

To determine the object shape the RGBD image is transformed into a 3D Point Cloud and sent to the the geometry recognition module. This module extracts the object position and the width, length, and height ($\boldsymbol{d}_{max}$).

In the subsequent step, the point cloud was processed using distance-based filtration. In this step, it was assumed that the object of interest is centred in the camera's field of view. Note that the camera was mounted close to the robot end-effector and the robot was able to move it and adjust the field of view. With this assumption, the average distance of all points to the camera can be calculated. The derived average, augmented by a threshold margin, was the limit for points in the vertical z-direction. All points

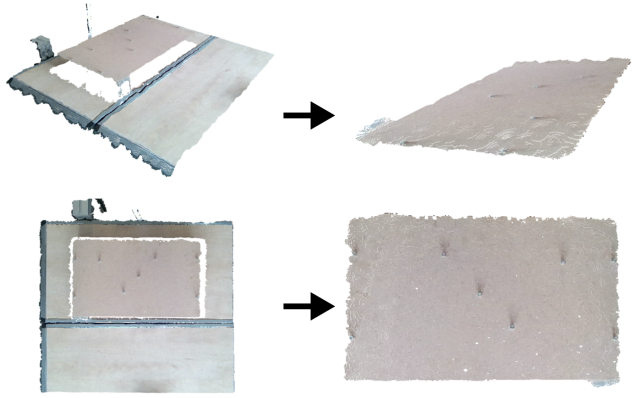

Fig. 4. Example of detecting a wooden plate and its geometry using a point cloud. The left column shows the detected point clouds of the plate and its surroundings from different perspectives. The right column shows cropped versions focusing on the object itself to measure its geometrical properties.

within this distance remained and formed a point cloud with distinct objects (Fig. 4, left). To extract the object of interest (Fig. 4, right) from the environment objects (i.e., the table upon which it is positioned) in the residual point cloud, the DBSCAN clustering algorithm was applied to identify distinct clusters [35].

The object of interest point cloud was then separated from the rest of the scenario and went through a noise filter to improve the efficiency of the following steps. RANSAC and the PCL library [36] were then used to segment the largest plane in the cloud. The extracted point cloud provides all the necessary information about the object geometry. Since the extracted point cloud of the object is in the camera frame, we have to transform it into the robot base frame to be able to use it for the robot stiffness calculation.

The relation of the object to the environment is determined by the configuration of environment support. If the object is lying on the environment, e.g., a plate resting on the edge of the environment as in Fig. 1), support is detected visually as the edge between the object and the environment. The identified support configuration in combination with the detected object geometry determines the stiffness map as shown in Fig. 3. We estimate object geometry and its relation to the environment before the robot enters into contact to be proactive and not reactive. However, these can also be monitored during the contact and updated online if there are changes in the environment.

IV. Experiments

To validate the efficacy of the developed semi-autonomous teleimpedance control method in real-world applications, a series of proof-of-concept experiments were undertaken. The teleoperation setup, illustrated in Fig. 1, featured a KUKA LBR iiwa as the remote robotic manipulator, a Force Dimension Sigma.7 as a haptic device, and an Intel Realsense D455 serving as an RGB-D camera. Since the workspace of the Sigma.7 haptic device is smaller than that of the LBR iiwa robot arm, we implemented a workspace re-indexing technique, which allowed the operator to shift the commanded position offset when Sigma.7 workspace limit was reached. The developed controller dynamically adjusted the impedance based on the robot's position relative to the object, considering factors such as material, shape, and mounting. We performed two tasks where impedance adaptation with respect to object geometry and material is important: engaging with bolts on a plate (500x300mm) supported on its two shorter sides and polishing a stripe (200x50mm) clamped on one side.

Before conducting the experiments, it was necessary to determine the maximum and minimum allowable stiffness. To achieve this, the setup was used to perform each task with a preset stiffness, and the bending of the object was measured. A maximum allowable bending was defined, and the stiffness was continuously increased while handling the object until the set limit was exceeded. Similarly, the minimum allowable stiffness was determined by gradually lowering the stiffness until the task could no longer be performed effectively.

A. Bolt-Engagement Task

In the bolt-engagement task, the primary objective was to use the robot to apply the necessary force to push bolts into a plate without causing damage. The robot's compliance was crucial to avoid plate damage due to excessive force. Simultaneously, insufficient impedance could result in position errors or inadequate force applied to the bolts.

To validate the proposed impedance control method, experiments were conducted on wood and metal plates. The robot end-effector position was controlled by a human operator in the Cartesian x-, y-, and z-axes. As the robot approached a predefined safety margin around the object (set to 10 cm), the impedance automatically adapted to its position relative to the detected object properties. The controller autonomously adjusted the stiffness as the operator performed the bolt-engagement task, resulting in dynamic impedance changes.

The results are shown in Fig. 5 and demonstrate the adaptive impedance adjustments based on the object properties. The operator started near the centre of the plate in the x-y position (first graph on top), which is its weakest point. This triggers an immediate drop in impedance to nearly the minimum allowable level (bottom graph). As the operator navigated the robot end-effector x-y position towards the first bolt, which was positioned farther from the plate's centre, the impedance progressively increased. While the first bolt was pressed on, the robot maintained the desired stiffness in the z-axis to facilitate the required force for task execution.

When the operator transitioned the robot end-effector x-y position the second bolt closer to the plate's centre (second graph on top), the stiffness was once again reduced by the robot (bottom graph). The stiffness reached the minimum allowable level as the operator transitioned the robot end-effector x-y position to the third bolt, as the centre of the plate was approached. Eventually, the stiffness subsequently increased as the operator moved the robot end-effector toward the fourth bolt (third graph on top) and the fifth bolt (fourth graph on top) since they were closer to the

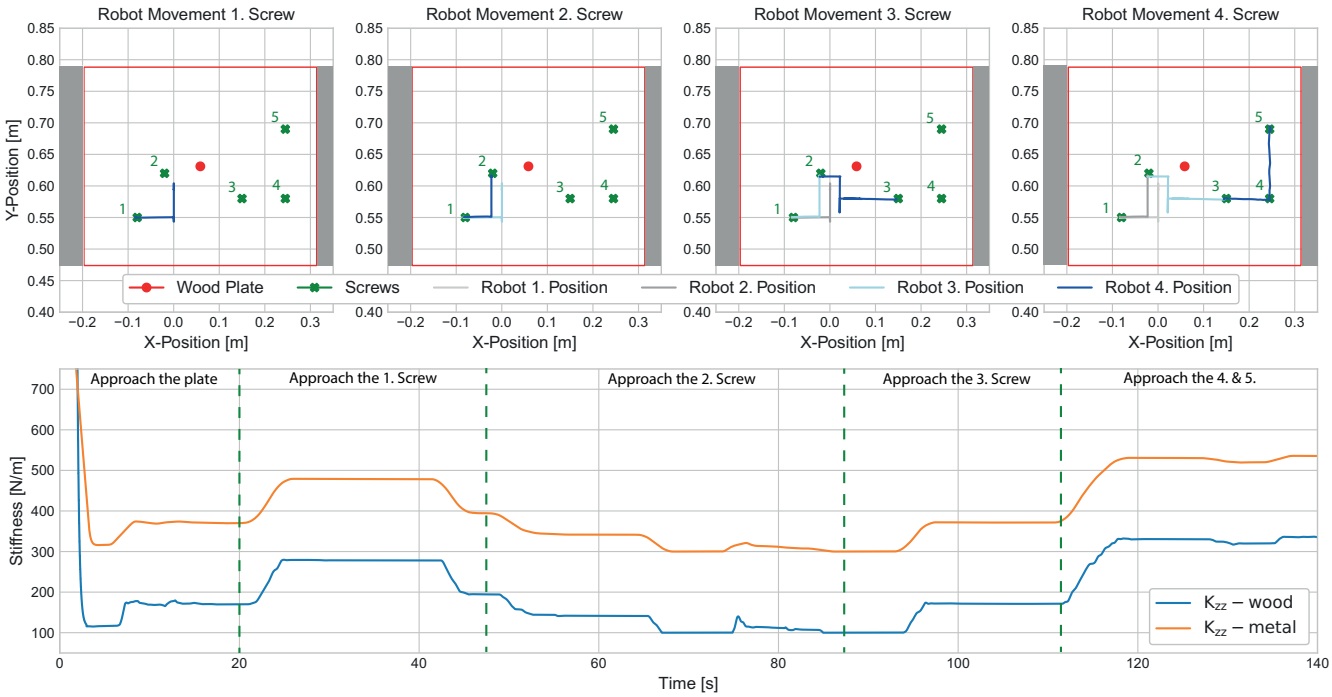

Fig. 5. Results of the bolt-engagement task for impedance adaption based on the material. The top graphs show the progression of the commanded position (blue and gray lines) relative to the plate (red outline). The plate was supported by the environment on two sides at $x = -0.2$ m and $x = 0.3$ m (scenario B in Fig. 3). The grey-shaded area represents the environment that supports the plate, while the red dot highlights the center of the plate, indicating its weakest point. The lower graph illustrates the robot's stiffness along the z-axis, perpendicular to the plate surface, showing how bolts were pressed into both wooden and metal plates. The dashed vertical lines denote the transitions between phases related to different bolt positions.

support. This dynamic modulation of stiffness aligns with the changing requirements of the task, showcasing the system's adaptability in response to the robot's movements.

B. Polishing Task

The objective of the polishing task was to demonstrate the algorithm's proficiency in handling impedance adaptations across multiple axes. Unlike the bolt-engagement task, where the robot primarily interacted from above the stripe, this experiment required the robot to engage with the object in all three axes, contingent on its position relative to the object. A notable distinction was the one-sided mounting of the object, necessitating lower stiffness at the open end due to its vulnerability to applied forces. Excessive force could potentially lead to over-bending and permanent damage to the object. Consequently, a more delicate approach was imperative on the open side compared to the clamped side. The experiment showcased object property and material detection using two distinct objects representing metal and wood, both sharing the same dimensions of 200x50x4 mm. For metal detection, the maximum permissible stiffness for interacting with the stripe was set at 700 N/m, while for wood it was set at 500 N/m. The minimum required stiffness for both materials was standardised at 150 N/m.

Figure 6 presents the results of the experiment conducted with the metal stripe. The graph depicts the robot's movement overlaid with the stiffness in the x-, y-, and z-axes. The initial step involved polishing the stripe from the top perpendicularly (first graph on top), with the mounting point illustrated by the red dot on the graph. At the onset, the operator positioned the robot end-effector at the end of the stripe, prompting an immediate drop in the z-axis stiffness to nearly the minimum allowed (bottom graph). As the robot moved toward the mounting location, the z-axis stiffness gradually increased to the maximum permitted until the robot shifted away from the stripe in the x-direction.

When the operator transitioned the robot end-effector position to polish perpendicularly on the x-axis (second graph on top), the z-axis stiffness increased to the default setting, while the x-axis stiffness decreased to the level suitable for the current position. Upon the robot's return to the end of the stripe (third graph on top), the x-axis stiffness decreased to the minimum allowed before progressing to the y-axis (fourth graph on top). This transition led to an increase in the x-axis stiffness to the default setting, coupled with adaptive adjustments in the y-direction. Given the relatively small lever in the y-axis with respect to the mounting point compared to the other axes, changes in stiffness in the y-axis were comparatively moderate. The nuanced adaptation illustrated the algorithm's ability to dynamically tailor stiffness based on the robot's position and task requirements during the polishing operation.

Here we compare our method to the method from the state-of-the-art [25], where there was only material recognition but no geometry. In our experiment, we used a metal plate with dimensions of 200x50x5 mm. Our method adapts the stiffness based on the geometry, ranging from a maximum of 700 N/m to a minimum of 150 N/m as the robot end-

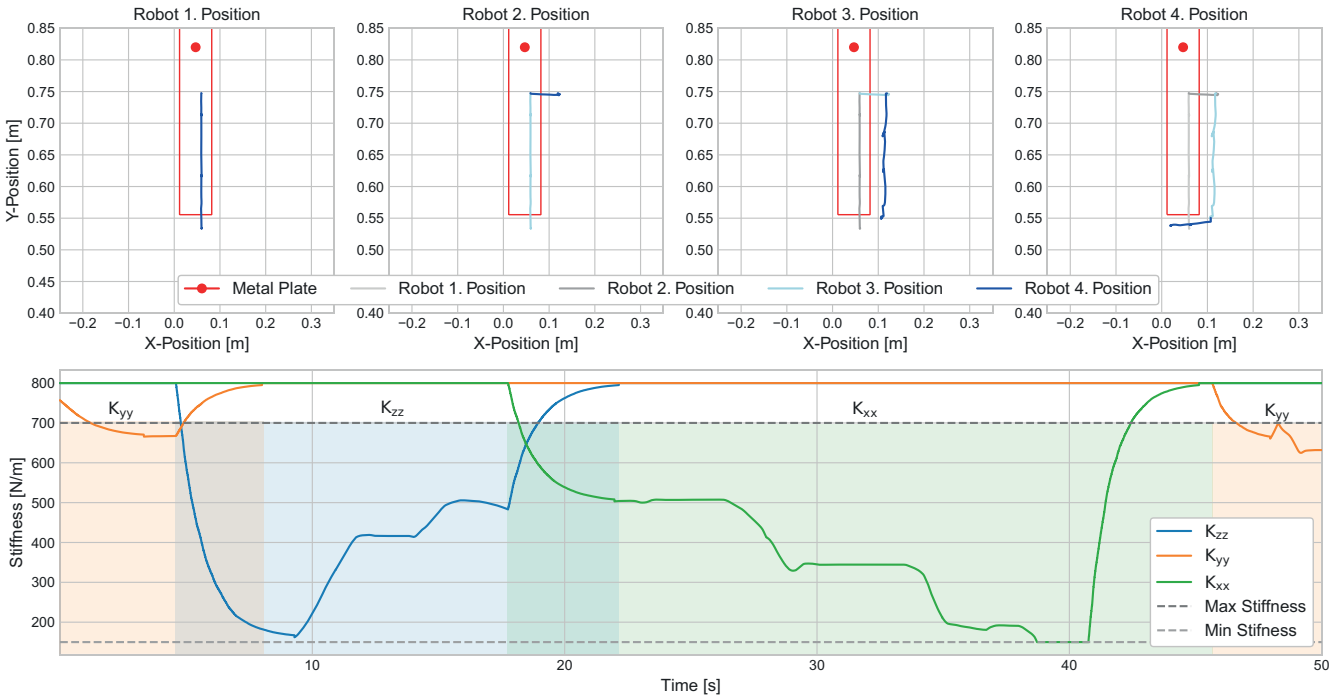

Fig. 6. Results of the metal stripe polishing task. The top graphs show the progression of the commanded position (blue and gray lines) relative to the stripe (red outline) and its mounting location (red dot). The bottom graph shows the robot stiffness in the x-, y-, and z-axis, with maximum stiffness applied only in the axis currently engaged in the task with the plate. The interaction along a specific axis is visualized with a colored background.

effector moves from the unsupported side of the plate to the supported one. On the other hand, using the average of our parameters, the method in [25] would then command a uniform stiffness of 425 N/m since it does not account for geometry dependence. We examine the bending of the object at two critical points: the end of the plate (y = 0.55 m) and the center point (y = 0.70 mm).

When the operator commands the reference position 20 mm below the plate, the corresponding force at both points for the method in [25] is 85 N. In contrast, for our method, the force is 30 N at the endpoint and 73 N at the center point. The resulting bending of the object is as follows. At the center of the plate, where there is still considerable structural strength, the bending with the method in [25] and our method is not that different (0.67 mm compared to 0.78 mm). However, at the unsupported side at the end of the plate where the object is the weakest, the method in [25] bends 6.12 mm, while our method bends only 2.20 mm. Thus, the proposed geometry-adaptive approach is safer since the previous approach poses a danger of damaging the plate by over-bending at weaker points.

V. Discussion

We developed a novel method for semi-autonomous teleimpedance using a vision-based algorithm to detect objects and their properties. The conducted experiments showed the applicability of the developed method in practical tasks such as polishing a stripe and engaging with bolts on a plate. The robot could autonomously adapt the impedance based on the object geometry and material while the human operator commanded the end-effector position in real-time. The experiments proved that the developed algorithm can adapt the impedance in different axes based on the detected objects, which highlights that the combination of object recognition, material detection, and shape clustering is an effective approach to impedance adaptation.

The trained models exhibited satisfactory precision in recognizing both objects and materials. In all of the performed experiments, the model could detect the object and material with a higher precision than 80%. Additionally, the clustering process yielded precise measurements, enabling accurate stiffness calculations. Consequently, the algorithm could adapt the desired impedance for the current position, and the transitions were smooth to not disturb the operator's movement control.

Practical implications of the proposed method may be in helping the human operators not to be overwhelmed during the teleoperation since it delegates the impedance control task to the robot. The human operator can dedicate more attention to the positioning task while the robot autonomously estimates and adapts the end-effector impedance. Moreover, it can help in situations where the operator may have limited visual feedback.

The MINC database has proven to be effective in recognizing materials. However, it may face difficulties when dealing with objects that are made of more than one material or have been painted or coated. This is because the current approach is primarily designed to identify materials in their "normal" colors. As a result, recognising painted or coated materials may be a challenge. In such cases, more precise material recognition methods will be essential, potentially requiring further development or utilisation of existing methodologies.

Furthermore, the development of the proposed method focused on low computational cost, primarily driven by real-time applicability. Increasing the low computational cost may improve estimations at the expense of real-time applicability.

Future development could explore non-linear impedance estimation and the integration of the current impedance estimation method with imitation learning approaches. While more complex imitation learning approaches might introduce challenges in stability, they also offer the potential to handle more complex objects.

REFERENCES

[1] K. Darvish, L. Penco, J. Ramos, R. Cisneros, J. Pratt, E. Yoshida, S. Ivaldi, and D. Pucci, "Teleoperation of humanoid robots: A survey," *IEEE Transactions on Robotics*, vol. 39, no. 3, pp. 1706–1727, 2023.

[2] W. Si, N. Wang, and C. Yang, "A review on manipulation skill acquisition through teleoperation-based learning from demonstration," *Cognitive Computation and Systems*, vol. 3, no. 1, pp. 1–16, 2021.

[3] A. Naceri, T. Schumacher, Q. Li, S. Calinon, and H. Ritter, "Learning optimal impedance control during complex 3d arm movements," *IEEE Robotics and Automation Letters*, vol. 6, no. 2, pp. 1248–1255, 2021.

[4] A. Ajoudani, N. Tsagarakis, and A. Bicchi, "Tele-impedance: Teleoperation with impedance regulation using a body–machine interface," *The International Journal of Robotics Research*, vol. 31, no. 13, pp. 1642–1656, 2012.

[5] L. Peternel and A. Ajoudani, "After a decade of teleimpedance: A survey," *IEEE Transactions on Human-Machine Systems*, vol. 53, no. 2, pp. 401–416, 2022.

[6] D. S. Walker, R. P. Wilson, and G. Niemeyer, "User-controlled variable impedance teleoperation," in *2010 IEEE International Conference on Robotics and Automation (ICRA)*, 2010, pp. 5352–5357.

[7] A. Ajoudani, C. Fang, N. Tsagarakis, and A. Bicchi, "Reduced-complexity representation of the human arm active endpoint stiffness for supervisory control of remote manipulation," *The International Journal of Robotics Research*, vol. 37, no. 1, pp. 155–167, 2018.

[8] S. Park, W. Lee, W. K. Chung, and K. Kim, "Programming by demonstration using the teleimpedance control scheme: Verification by an semg-controlled ball-trapping robot," *IEEE Transactions on Industrial Informatics*, vol. 15, no. 2, pp. 998–1006, 2018.

[9] C. Yang, C. Zeng, C. Fang, W. He, and Z. Li, "A dmps-based framework for robot learning and generalization of humanlike variable impedance skills," *IEEE/ASME Transactions on Mechatronics*, vol. 23, no. 3, pp. 1193–1203, 2018.

[10] J. Li, G. Li, Z. Chen, and J. Li, "A novel emg-based variable impedance control method for a tele-operation system under an unstructured environment," *IEEE Access*, vol. 10, pp. 89 509–89 518, 2022.

[11] E. Hocaoglu and V. Patoglu, "semg-based natural control interface for a variable stiffness transradial hand prosthesis," *Frontiers in Neurorobotics*, vol. 16, p. 789341, 2022.

[12] S. Buscaglione, N. L. Tagliamonte, G. Ticchiarelli, G. Di Pino, D. Formica, and A. Noccaro, "Tele-impedance control approach using wearable sensors," in *2022 44th Annual International Conference of the IEEE Engineering in Medicine & Biology Society (EMBC)*. IEEE, 2022, pp. 2870–2873.

[13] H. Ahn, Y. Michel, T. Eiband, and D. Lee, "Vision-based approximate estimation of muscle activation patterns for tele-impedance," *IEEE Robotics and Automation Letters*, vol. 8, no. 8, pp. 5220–5227, 2023.

[14] L. Peternel, T. Petrič, and J. Babič, "Robotic assembly solution by human-in-the-loop teaching method based on real-time stiffness modulation," *Autonomous Robots*, vol. 42, no. 1, pp. 1–17, 2018.

[15] V. R. Garate, S. Gholami, and A. Ajoudani, "A scalable framework for multi-robot tele-impedance control," *IEEE Transactions on Robotics*, vol. 37, no. 6, pp. 2052–2066, 2021.

[16] A. Giammarino, J. M. Gandarias, and A. Ajoudani, "An open tele-impedance framework to generate data for contact-rich tasks in robotic manipulation," in *2023 IEEE International Conference on Advanced Robotics and Its Social Impacts (ARSO)*. IEEE, 2023, pp. 140–146.

[17] J. Schol, J. Hofland, C. J. Heemskerk, D. A. Abbink, and L. Peternel, "Design and evaluation of haptic interface wiggling method for remote commanding of variable stiffness profiles," in *2021 20th International Conference on Advanced Robotics (ICAR)*, 2021, pp. 172–179.

[18] G. Gourmelen, B. Navarro, A. Cherubini, and G. Ganesh, "Human guided trajectory and impedance adaptation for tele-operated physical assistance," in *2021 IEEE/RSJ International Conference on Intelligent Robots and Systems (IROS)*, 2021, pp. 9276–9282.

[19] J. Buchli, F. Stulp, E. Theodorou, and S. Schaal, "Learning variable impedance control," *The International Journal of Robotics Research*, vol. 30, no. 7, pp. 820–833, 2011.

[20] F. J. Abu-Dakka and M. Saveriano, "Variable impedance control and learninga review," *Frontiers in Robotics and AI*, vol. 7, p. 590681, 2020.

[21] R. Wu and A. Billard, "Learning from demonstration and interactive control of variable-impedance to cut soft tissues," *IEEE/ASME Transactions on Mechatronics*, vol. 27, no. 5, pp. 2740–2751, 2021.

[22] C. Yang, G. Ganesh, S. Haddadin, S. Parusel, A. Albu-Schaeffer, and E. Burdet, "Human-like adaptation of force and impedance in stable and unstable interactions," *IEEE transactions on robotics*, vol. 27, no. 5, pp. 918–930, 2011.

[23] A. Brygo, I. Sarakoglou, N. Tsagarakis, and D. G. Caldwell, "Tele-manipulation with a humanoid robot under autonomous joint impedance regulation and vibrotactile balancing feedback," in *2014 IEEE-RAS International Conference on Humanoid Robots*. IEEE, 2014, pp. 862–867.

[24] Y. Michel, R. Rahal, C. Pacchierotti, P. R. Giordano, and D. Lee, "Bilateral teleoperation with adaptive impedance control for contact tasks," *IEEE Robotics and Automation Letters*, vol. 6, no. 3, pp. 5429–5436, 2021.

[25] Y.-C. Huang, D. A. Abbink, and L. Peternel, "A semi-autonomous tele-impedance method based on vision and voice interfaces," in *2021 20th International Conference on Advanced Robotics (ICAR)*, 2021, pp. 180–186.

[26] K. Haninger, C. Hegeler, and L. Peternel, "Model predictive impedance control with gaussian processes for human and environment interaction," *Robotics and Autonomous Systems*, vol. 165, p. 104431, 2023.

[27] F. Xie, Z. Chong, X.-J. Liu, H. Zhao, and J. Wang, "Precise and smooth contact force control for a hybrid mobile robot used in polishing," *Robotics and Computer-Integrated Manufacturing*, vol. 83, p. 102573, 2023.

[28] K. Zhou, S. Wang, R. Zhou, and B. Wang, "Admittance control design and system testing of industrial robot polishing operation," *Proceedings of the Institution of Mechanical Engineers, Part B: Journal of Engineering Manufacture*, vol. 237, no. 10, pp. 1538–1552, 2023.

[29] D. Mironov, M. Altamirano, H. Zabihifar, A. Liviniuk, V. Liviniuk, and D. Tsetserukou, "Haptics of screwing and unscrewing for its application in smart factories for disassembly," in *Haptics: Science, Technology, and Applications: 11th International Conference, EuroHaptics 2018, Pisa, Italy, June 13-16, 2018, Proceedings, Part II 11*. Springer, 2018, pp. 428–439.

[30] N. Hogan, "Impedance control: An approach to manipulation," *Journal of dynamic systems, measurement, and control*, vol. 107, no. 1, pp. 1–24, 1985.

[31] A. Albu-Schaffer, C. Ott, U. Frese, and G. Hirzinger, "Cartesian impedance control of redundant robots: Recent results with the dlr-light-weight-arms," in *2003 IEEE International Conference on Robotics and Automation (ICRA)*, vol. 3, 2003, pp. 3704–3709.

[32] J. Redmon, S. Divvala, R. Girshick, and A. Farhadi, "You only look once: Unified, real-time object detection," in *Proceedings of the IEEE conference on computer vision and pattern recognition*, 2016, pp. 779–788.

[33] B. Dwyer, J. Nelson, J. Solawetz *et al.*, "Roboflow," 2022, computer Vision Software. [Online]. Available: https://roboflow.com

[34] S. Bell, P. Upchurch, N. Snavely, and K. Bala, "Material recognition in the wild with the materials in context database," in *Proceedings of the IEEE conference on computer vision and pattern recognition*, 2015, pp. 3479–3487.

[35] A. Ram, S. Jalal, A. S. Jalal, and M. Kumar, "A density based algorithm for discovering density varied clusters in large spatial databases," *International Journal of Computer Applications*, vol. 3, no. 6, 2010.

[36] R. B. Rusu and S. Cousins, "3d is here: Point cloud library (pcl)," in *2011 IEEE International Conference on Robotics and Automation (ICRA)*. IEEE, 2011, pp. 1–4.